Cell Systems, Volume *6*

Supplemental Information

Compensation of Signal Spillover in Suspension and Imaging Mass Cytometry

Stéphane Chevrier, Helena L. Crowell, Vito R.T. Zanotelli, Stefanie Engler, Mark D. Robinson, and Bernd Bodenmiller

Cell Systems, Volume *6*

Supplemental Information

Compensation of Signal Spillover in Suspension and Imaging Mass Cytometry

Stéphane Chevrier, Helena L. Crowell, Vito R.T. Zanotelli, Stefanie Engler, Mark D. Robinson, and Bernd Bodenmiller

Supplemental information

Compensation of signal spillover in suspension and imaging mass cytometry

Stéphane Chevrier*, Helena Crowell*, Vito R.T. Zanotelli*, Stefanie Engler, Mark D. Robinson, and Bernd Bodenmiller

* These authors contributed equally

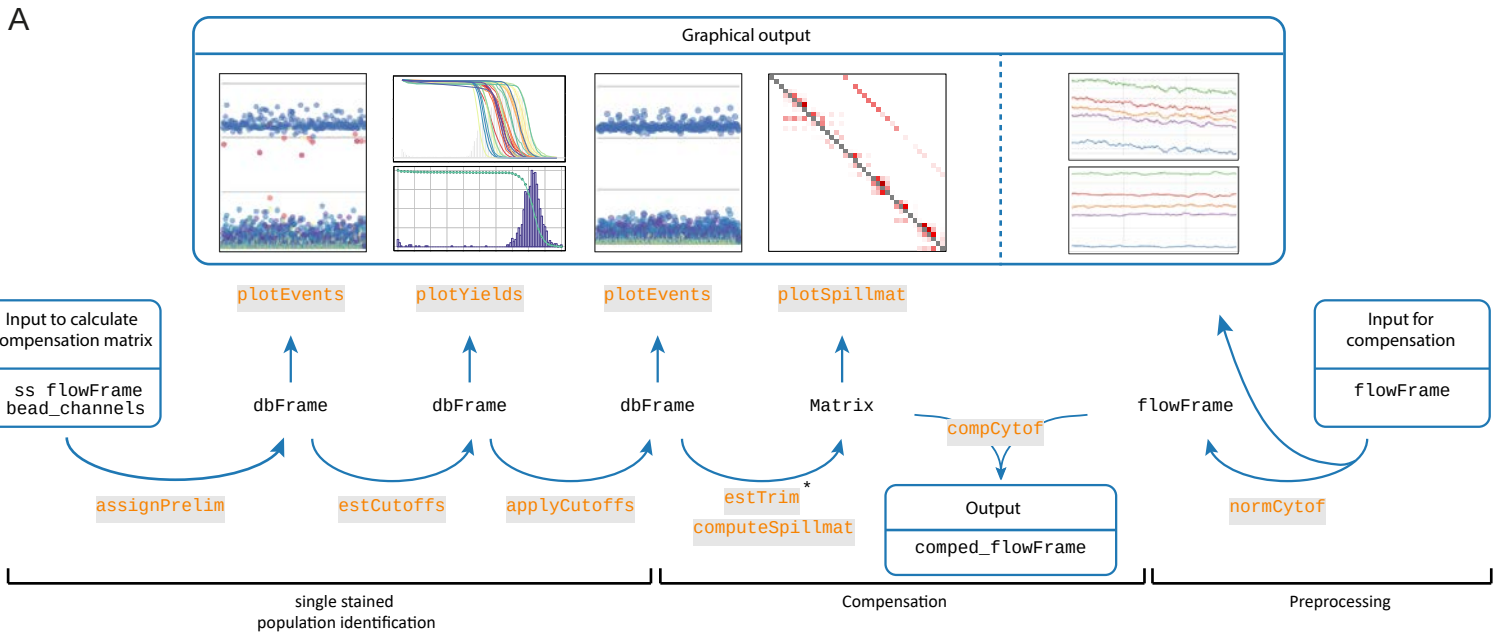

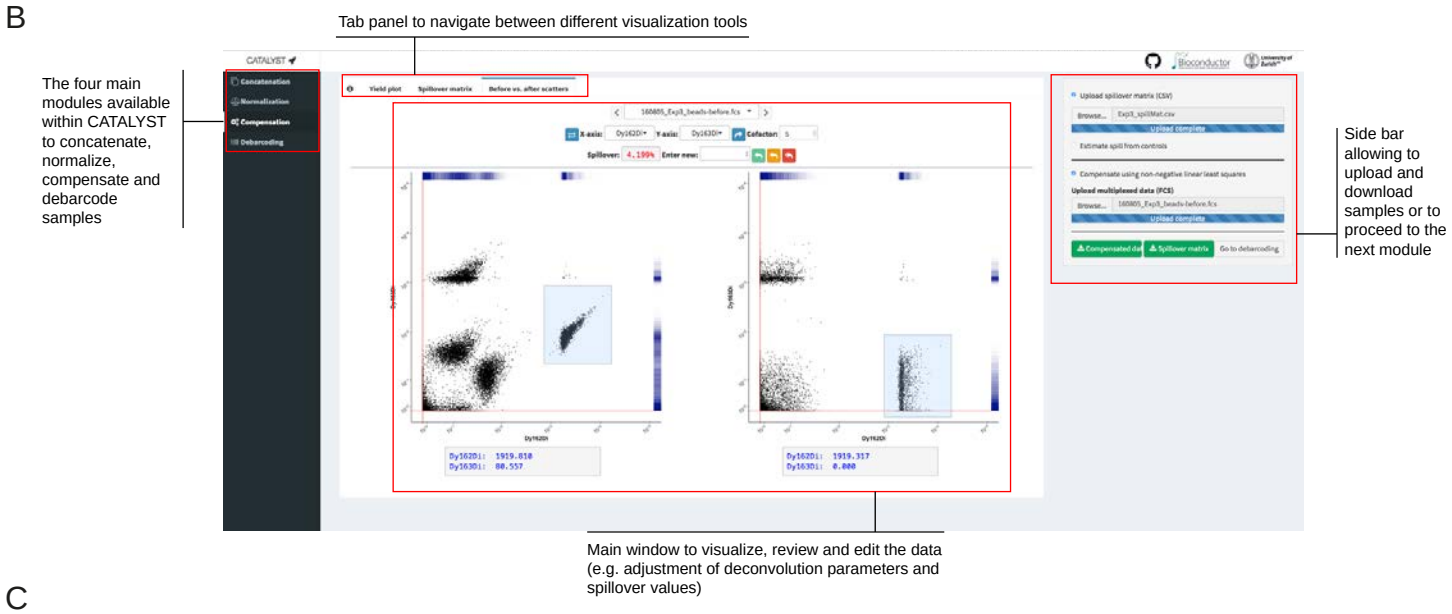

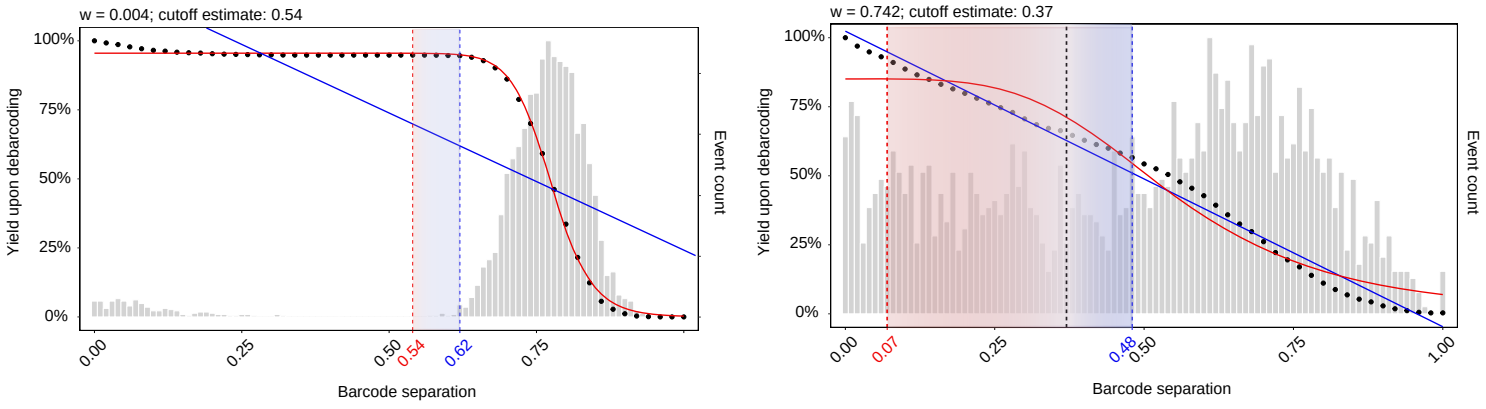

Figure S1. Description of the main functions of the CATALYST package. Related to Figure 1.

(A) Schematic of the workflow used in the CATALYST package to generate a compensated file based on beads stained with single antibodies. The graphical outputs generated during the process are indicated above the steps.
(B) Screen shot depicting the main features available with the Shiny app. The compensation module is used as an example.
(C) Description of the automatic cutoff estimation for each individual population. The bar graphs indicate the distribution of cells relative to the barcode distance, and the dotted line corresponds to the yield upon debarcoding as a function of the applied separation cutoff. Data were fitted with a linear regression (blue line) and a three parameter log-logistic function (red line). The cutoff estimate is defined as the mean of estimates derived from both fits, weighted with the goodness of the respective fit (see STAR Methods).

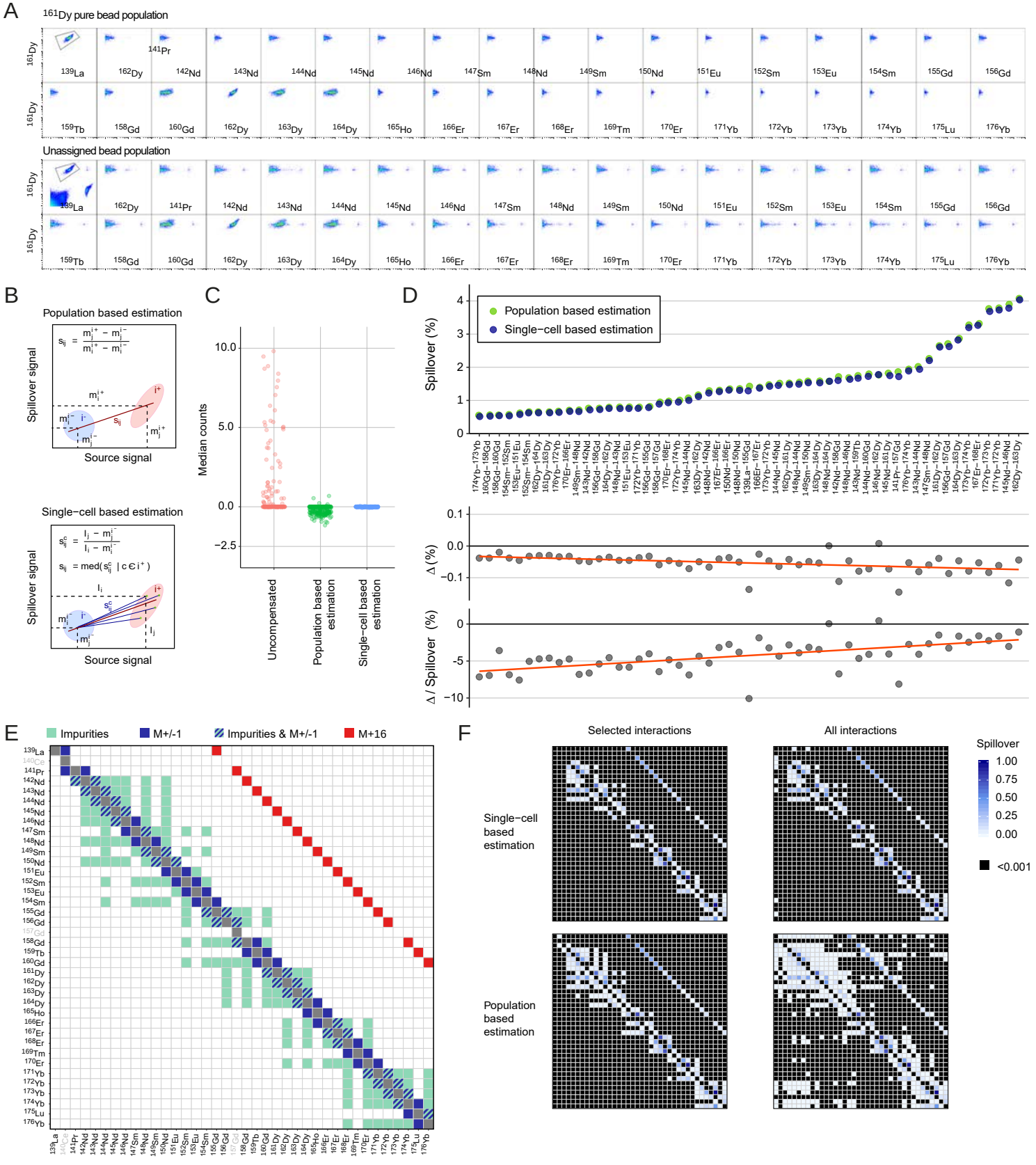

Figure S2. Description of the specificities of spillover matrix calculation for mass cytometry data. Related to Figure 2.

(A) Scatter plot showing the bead purity upon deconvolution using the ^{161}Dy population as a representative exampleand compared to unassigned beads. The top left graph of each panel corresponds to the total population; the other plots show the profile of the ^{161}Dy^{+}^{162}Dy^{-} population as gated in the first plot. The scale covers the range between 0 and 10^4 counts.
(B) Scheme describing spillover estimates at the population level (upper panel) and at the single-cell level (lower panel).
(C) Dot plots showing the median counts in each channel potentially affected by spillover for beads compensated based on population estimates versus single-cell estimates compared to uncompensated data.
(D) Plots showing the spillover in percent for the main interactions as assessed at the population level and at the single-cell level (top panel) and the absolute difference (middle panel) and the relative difference (lower panel) in spillover percentages.
(E) Spillover matrix showing the interactions estimated by default in CATALYST. Only those interactions expected to occur based on impurities, abundance sensitivity, and oxidation are taken into consideration.
(F) Spillover matrix calculated for expected interactions versus all interactions using single-cell estimates (upper panels) versus population estimates (lower panels).

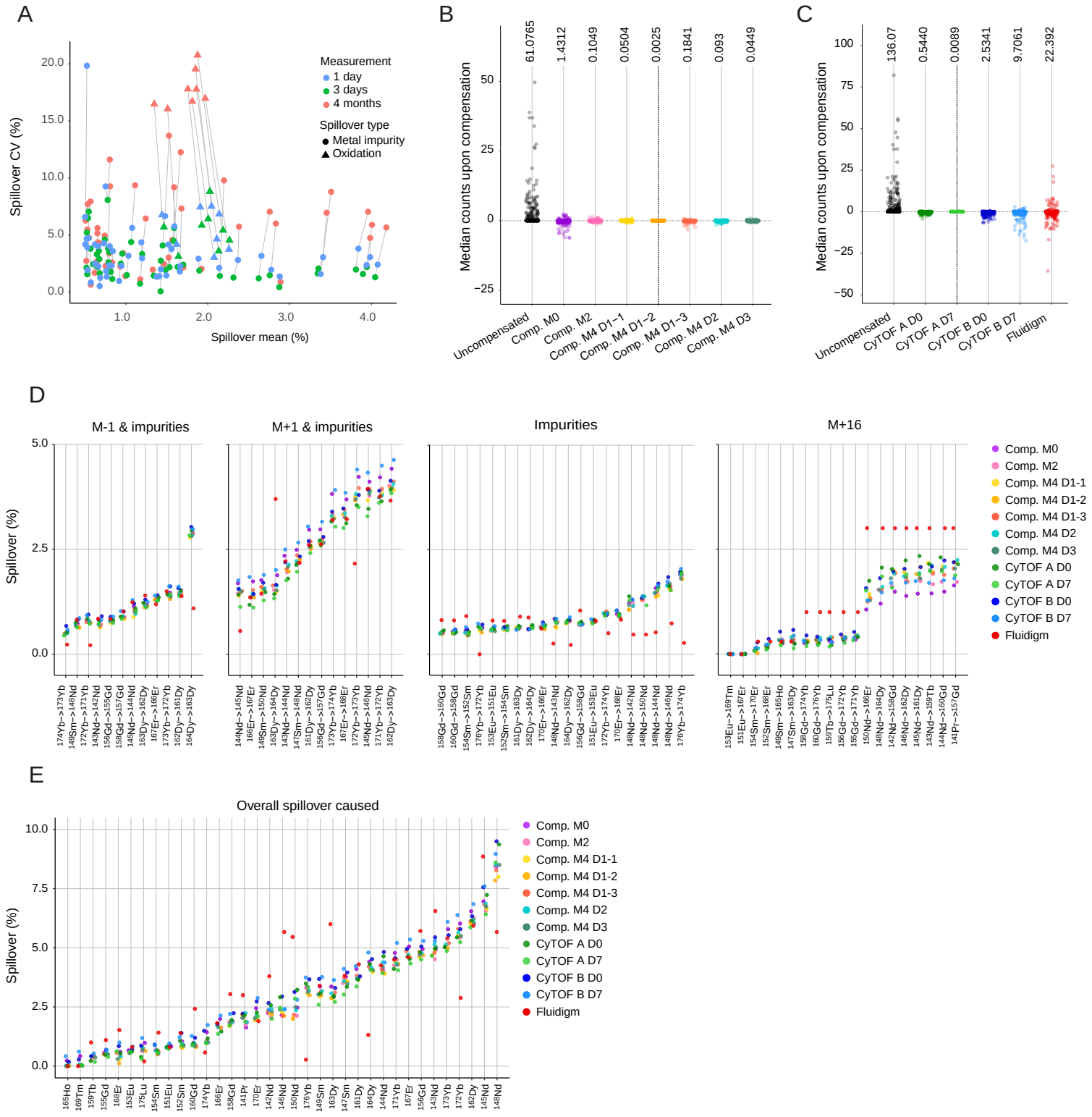

Figure S3. Compensation matrix stability over stainings, measurements, and instruments. Related to Figure 2.

(A) Scatter plot displaying the means and standard deviations of the spillover measured the same day (blue), after three days (green), and after four months (red). The origin of spillover (metal impurity versus oxidation) is indicated.
(B) Spillovers observed in single-stained beads in absence of compensation and upon compensation with each of seven different matrices acquired at the indicated time points are displayed as a dot plot. For each dataset, the average sum of squares is shown on top of the graph.
(C) Spillovers observed in single-stained beads without and upon compensation with each of four matrices acquired at the indicated time points on the indicated instruments are displayed as a dot plot. The compensation performed with the compensation matrix provided by Fluidigm is also shown. For each dataset, the average sum of squares is shown on top of the graph.
(D) Spillovers assessed for the individual relationships for the seven matrices acquired over 4 months, for the four matrices acquired on two different machines, and for the theoretical matrix provided by Fluidigm. Data are shown for M-1 and impurities (mean interaction > 0.5%), M+1 and impurities (>0.5%), impurities (>0.5%), and M+16 (all interactions).
(E) Scatter plot showing the total amount of spillover in each individual channel for the seven matrices acquired over 4 months, for the four matrices acquired on two different machines, and for the theoretical matrix provided by Fluidigm.

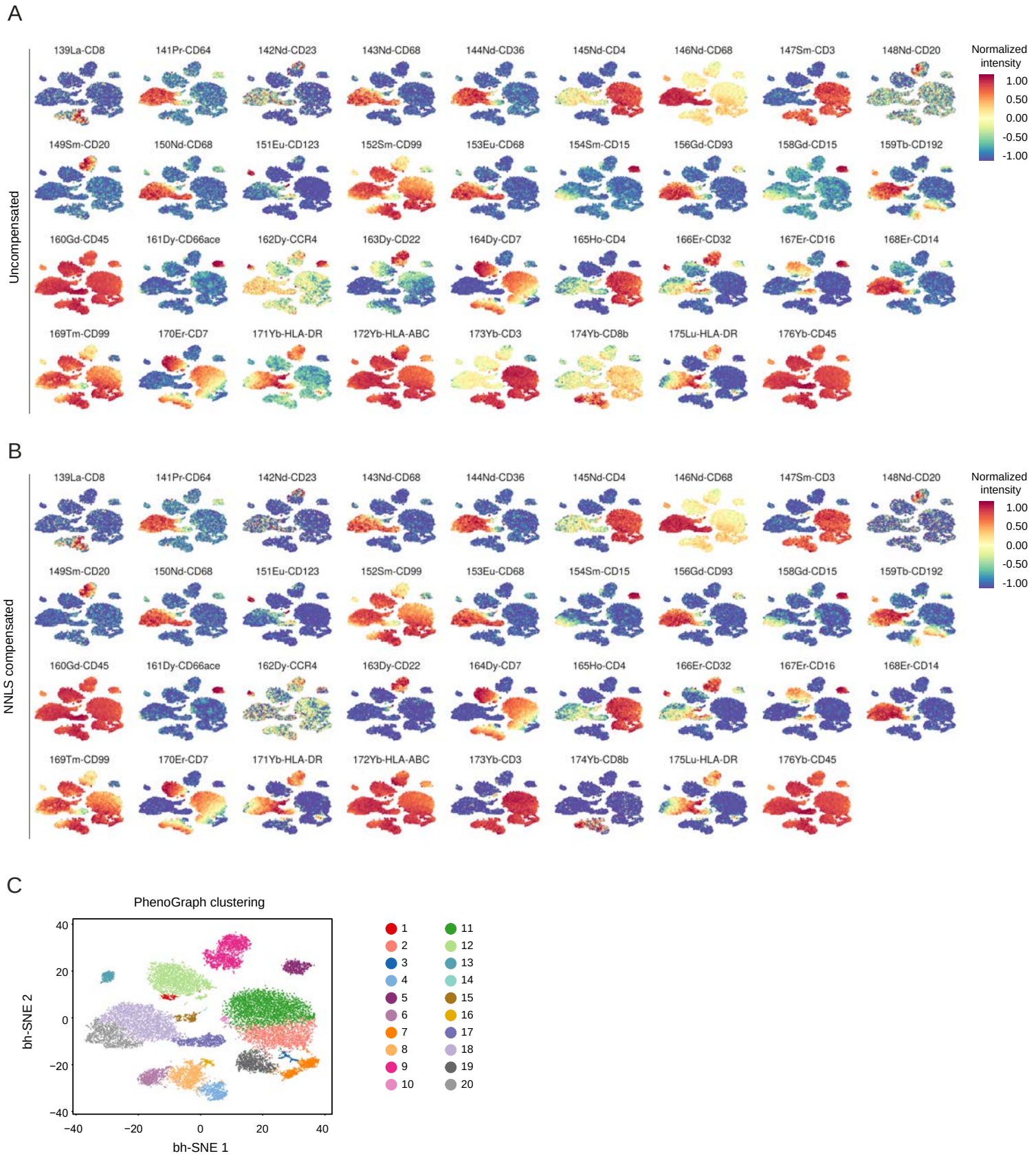

Figure S4. Interpretation of t-SNE maps in presence or absence of compensation. Related to Figure 3.

(A) t-SNE maps displaying data on a subset of 20,000 PBMCs analyzed with our 36-antibody panel are colored by marker expression for all the antibodies included in the analysis in absence of compensation.
(B) t-SNE map generated as indicated in A after compensation based on NNLS.
(C) t-SNE map colored by PhenoGraph clusters identified on uncompensated data.

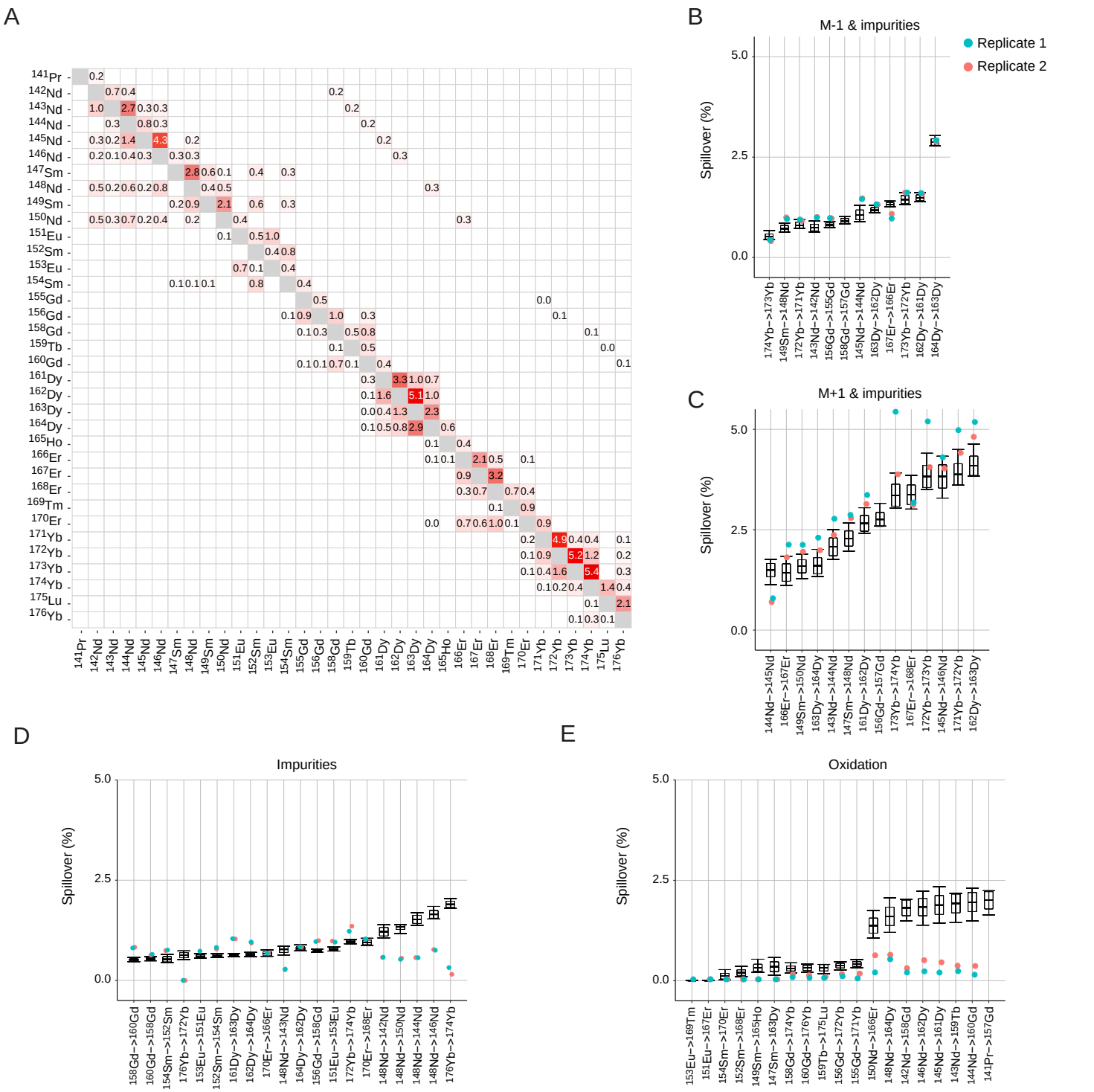

Figure S5. Compensation matrix for IMC. Related to Figure 4.

(A) Spillover matrix calculated based on single isotope containing pixels. Values on the diagonals are one. Spillover is calculated only in potentially affected channels (Figure S2D). Numbers in the squares indicate percentages of spillover by channels in rows into channels in columns.
(B-E) Signal interference for the indicated interactions shown for two independent IMC measurements of single isotopes spotted on a slide. Box plots show the spillover values obtained across the 11 replicates performed in flow mass cytometry as described in Figure 5D.

Table S1. Antibody panel used to establish a compensation workflow to correct for spillover in mass cytometry. Related to Figure 1, 2 and 3.

List of the 36 antibodies used in the panel in this study and information regarding the metal, the mass, the antigen, and the clone. Asterisks indicate antibody grouping for the experiment shown in Figure 2C.

Number	Metal	Isotope	Antigen	Clone	Isotype
1	La	139	CD8a*	RPA-T8	Mouse IgG1, κ
2	Pr	141	CD64*	10.1	Mouse IgG1, κ
3	Nd	142	CD23	EBVCS-5	Mouse IgG1, κ
4	Nd	143	CD68*	Y1/82A	Mouse IgG2b, κ
5	Nd	144	CD36	5-271	Mouse IgG2a, κ
6	Nd	145	CD4*	RPA-T4	Mouse IgG1, κ
7	Nd	146	CD68	KP1	Mouse IgG1, κ
8	Sm	147	CD3*	UCHT1	Mouse IgG1, κ
9	Nd	148	CD20	H1(FB1)	Mouse BALB/c IgG2a, κ
10	Sm	149	CD20	L26	Mouse / IgG2a, kappa
11	Nd	150	CD68*	Y1/82A	Mouse IgG2b, κ
12	Eu	151	CD123	6H6	Mouse IgG1, κ
13	Sm	152	CD99	HCD99	Mouse IgG2a, κ
14	Eu	153	CD68*	Y1/82A	Mouse IgG2b, κ
15	Sm	154	CD15*	HI98	Mouse IgM, κ
16	Gd	155	CD273	MIH18	Mouse IgG1, κ
17	Gd	156	CD93*	R139	Mouse BALB/c IgG2b, κ
18	Gd	158	CD15	HI98	Mouse IgM, κ
19	Tb	159	CD192	K036C2	Mouse IgG2a, κ
20	Gd	160	CD45*	HI30	Mouse IgG1, κ
21	Dy	161	CD66a/c/e	ASL-32	Mouse IgG2b, κ
22	Dy	162	CXCR4*	12G5	Mouse IgG2a, κ
23	Dy	163	CD22	HIB22	Mouse IgG1, κ
24	Dy	164	CD7*	M-T701	Mouse BALB/c IgG1, κ
25	Ho	165	CD4	RPA-T4	Mouse IgG1, κ
26	Er	166	CD32	FUN-2	Mouse IgG2b, κ
27	Er	167	CD16*	3G8	Mouse IgG1, κ
28	Er	168	CD14	RMO52	IgG2a κ, mouse
29	Tm	169	CD99*	HCD99	Mouse IgG2a, κ
30	Er	170	CD7	M-T701	Mouse BALB/c IgG1, κ
31	Yb	171	HLA-DR*	L243	Mouse IgG2a, κ
32	Yb	172	HLA-ABC	W6/32	Mouse IgG2a, κ
33	Yb	173	CD3*	UCHT1	Mouse IgG1, κ
34	Yb	174	CD8b	SIDI8BEE	Mouse IgG1, κ
35	Lu	175	HLA-DR*	L243	Mouse IgG2a, κ
36	Yb	176	CD45	HI30	Mouse IgG1, κ